Poly(ethylene oxide) Crystallization within a One-Dimensional Defect-Free Confinement on the Nanoscale

Ming-Siao Hsiao,[†] William Y. Chen,[†] Joseph X. Zheng,[†] Ryan M. Van Horn,[†] Roderic P. Quirk,[†] Dimitri A. Ivanov,[‡] Edwin L. Thomas,[§] Bernard Lotz,*[,||] and Stephen Z. D. Cheng*[,†]

Maurice Morton Institute and Department of Polymer Science, The University of Akron, Akron, Ohio 44325-3909; Institut de Chimie des Surfaces et Interfaces, UPR CNRS 9069, 15 rue Jean Starcky, B.P. 2488, 68057 Mulhouse Cedex, France; Department of Materials Science and Engineering, Massachusetts Institute and Technology, Cambridge, Massachusetts 02139; and Institut Charles Sadron, 23, Rue du Loess, Strasbourg 67034, France

Received March 25, 2008; Revised Manuscript Received May 9, 2008

ABSTRACT: A new approach was designed to study polymer crystallization in a one-dimensional (1D), defect-free, nanoscale confinement utilizing single crystals of poly(ethylene oxide)-*block*-polystyrene (PEO-*b*-PS) diblock copolymers as templates. The single crystals grown in dilute solution consisted of a PEO single crystal layer sandwiched between two PS layers formed by the tethered PS blocks on the PEO single crystal top and bottom basal surfaces. Transition behaviors of PEO-*b*-PS single crystals were investigated using differential scanning calorimetry, transmission electron microscopy, and atomic force microscopy. It was observed that the glass transition temperature of PS blocks in a thin film with a thickness of 7.2 nm is 71 °C, which is higher than the melting temperature of a PEO single crystal with a thickness of 7.9 nm (57 °C). Therefore, the PEO single crystal could be melted, and the PEO blocks could recrystallize in between these two vitrified PS layers when the temperature is brought down to generate sufficient supercooling. This recrystallization process of the PEO blocks was thus carried out in a 1D lamellar confinement without any defects. After the recrystallization, the crystal orientation change of the PEO crystals at different recrystallization temperatures (T_{rx}) was monitored using electron diffraction (ED). First, it was found that the PEO blocks could not recrystallize at $T_{rx} > -5$ °C, indicating absence of heterogeneous nucleation in the PEO blocks. This T_{rx} of −5 °C corresponds to the starting temperature for homogeneous nucleation of PEO as reported previously. Second, crystallographic analyses of the ED obtained from the recrystallized PEO blocks show that for $T_{rx} < -20$ °C the *c*-axis, and thus the PEO small crystals, possess a random orientation. When -20 °C $\leq T_{rx} < -5$ °C, the *c*-axis of the PEO crystals is parallel to the glassy PS basal plane and aligned with the *a**- or *b*-axis of the original PEO-*b*-PS single crystal grown in dilute solution. The self-seeding technique was used for $T_{rx} > -5$ °C to create heterogeneous nucleation. Here, the *c*-axis of PEO crystals was inclined with respect to the vitrified PS lamellar normal at an angle of about 26°.

Introduction

Many ways of constructing nanoconfined environments have been utilized to study phase transitions of polymers in low-dimensional spaces, be they one-, two-, or three-dimensionally small. When materials, such as polymers, form ordered structures in these small spaces, they possess a large surface-to-volume ratio. Therefore, phase transitions of these materials in the confined environments may differ from those in the bulk.[1–14] However, to generate a perfect, defect-free, and precisely controlled confinement is always a difficult task. Among different ways to construct these confinements, the use of nanophase-separated diblock copolymers has been extensively utilized. It is known that under large mechanical shearing diblock copolymers with two strongly phase-separated blocks form different phase structures ranging from lamellae, to double gyroids (also hexagonally perforated layers), to cylinders, and to spheres, depending on the volume fraction of the blocks.[15,16] When one of the blocks is crystallizable and its volume fraction is equal to or smaller than 50%, the crystalline materials can be confined in nanometer size domains if its melting temperature is lower than the order−disorder transition temperature (T_{ODT}) of the diblock copolymer (for upper critical solution temperature systems) and the glass transition temperature of the amorphous block (T_g).[17–37] Also, the crystallization kinetics are determined by nucleation within the confined domain.

The purpose of the mechanical shear is to generate macroscopic single domains of the phase structures with a uniform structural orientation. After crystallization of the crystallizable blocks, the crystal orientation changes in the nanodomains at different crystallization temperatures (T_x) can be investigated via wide-angle X-ray diffraction (WAXD) techniques.[26,27,30–37] However, in almost all of the samples generated by the mechanical shear, defects with edge and screw dislocations in the lamellar structure always form. This is because the mechanical shear usually generates grains and subgrains which intrinsically create defects.[38–40] These defects commonly release the size confinement and affect the crystallization kinetics and associated structural evolutions. As in the case of poly(ethylene oxide)-*block*-polystyrene (PEO-*b*-PS) with a lamellar structure, the confinement is compromised due to the formation of defects. This will affect the results of the crystallization kinetics of the PEO blocks due to "cross-talking" between neighboring PEO layers.[41] An ideal case in constructing a one-dimensionally (1D) confined environment should thus be a single crystallizable layer (such as PEO blocks) sandwiched by two glassy layers (such as PS blocks), all of which are on the nanoscale. If these two thin PS layers possess a T_g^{PS} which is higher than the T_m^{PEO} of PEO crystals, the PEO crystal can thus be melted and recrystallized within its nanolayer. In this case, the confinement direction is along the lamellar layer normal.

* To whom correspondence should be addressed. E-mail: scheng@uakron.edu; lotz@ics.u-strasbg.fr.
[†] The University of Akron.
[‡] UPR CNRS 9069.
[§] Massachusetts Institute and Technology.
[||] Institut Charles Sadron.

10.1021/ma8006619 CCC: $40.75
Published on Web 06/06/2008

The experimental techniques used to prepare samples in the past remain a critical issue: How do we construct a PS/PEO/PS sandwiched layer system having each layer thickness on the nanometer length scale? Commonly, the Langmuir−Blodgett technique is used to make structurally ordered thin films for amphiphilic small molecules, oligomers, and copolymers with highly asymmetric compositions.[42–44] However, it is not suitable for the high molecular weight copolymers which lack asymmetric compositions. In addition, there are issues of density fluctuations in the layers that may arise. Spin-coating and solution-casting are popular methods used to make layers with nanometer to submicrometer thicknesses on substrates. Yet, dewetting and uncontrolled layer compositions are issues when making the sandwiched layer system.[45–47]

In this publication, we propose to use PEO-*b*-PS diblock copolymers and grow single crystals in dilute solution to construct a precisely controlled, nanoconfined, lamellar geometry. The single crystals consist of a PEO nanolayer sandwiched by two PS glassy nanolayers. As reported previously, these PEO-*b*-PS diblock copolymers can form single crystals laterally bounded by four (120) crystal growth planes in, for example, chlorobenzene/octane mixed solvent or other solvents.[48–51] The two PS layers cover both of the PEO crystal basal surfaces; therefore, the overall PEO-*b*-PS single crystal consists of one layer of PEO crystal "sandwiched" in between two PS layers. This lamella provides a single confined domain of PEO without the possibility of morphological defects as seen in the bulk sample. Thus, a defect-free environment is created. Using this "sandwiched" system, it may be possible to have a situation where recrystallization is possible as previously described. We can thus carry out the investigation of the PEO block recrystallization and crystal orientation at different recrystallization temperatures (T_{rx}) in a 1D defect-free lamellar confinement.

Experimental Section

Materials and Samples. A PEO-*b*-PS diblock copolymer having $M_n^{PEO} = 11$K g/mol and $M_n^{PS} = 17$K g/mol was used for a majority of this study. Another PEO-*b*-PS block copolymer with different molecular weights ($M_n^{PS} = 3.8$K g/mol, and $M_n^{PEO} = 67$K g/mol) and a homo-PEO sample (50K g/mol) were also used for comparison. The detailed sequential living anionic polymerization of the samples was described previously.[52] For the major sample used, the M_n^{PS} precursors of 17K g/mol and a polydispersity of 1.02 were characterized by size exclusion chromatography (SEC) using polystyrene standards. The M_n^{PEO} blocks of 11K g/mol were determined by proton nuclear magnetic resonance results. The polydispersity in the final diblock copolymer, which was 1.07, was determined by SEC using the universal calibration.

Single crystals of PEO-*b*-PS were grown in a mixed solvent of chlorobenzene and octane with a 1:1 weight ratio and a concentration of 0.01 wt %. The polymer samples were dissolved at $T_d = 42$ °C in a temperature-controlled oil bath. The self-seeding procedure was utilized to achieve a large number of crystals with a uniform size.[48,53] The homogeneous polymer solution was crystallized at room temperature and reheated to a seeding temperature 1 °C lower than the T_d and kept there for 20 min. The sample was then quickly cooled to a preset T_x in an isothermal oil bath to grow single crystals. Note that only lamellae are formed in solution excluding any ordered phase morphologies observed in the sheared bulk state of the block copolymer. Droplets of the solution containing the lamellae were deposited on a silicon wafer surface. The mixed solvent was evaporated before atomic force microscopy (AFM) observations. For transmission electron microscopy (TEM), a drop of the crystal suspension was deposited onto a carbon film supported by a copper grid, and the solvent was evaporated.

Equipment and Experiments. Differential scanning calorimetry (DSC) experiments were carried out on a Perkin-Elmer PYRIS Diamond DSC with an Intracooler 2P apparatus to measure the T_m^{PEO} of PEO layer and the T_g^{PS} of PS layer in PEO-*b*-PS single crystals. The fully crystallized single crystal mats with a typical weight of 1.0 mg were heated at 10 °C/min. The endothermic peak temperature was taken as the T_m^{PEO}. The weight percent crystallinity was calculated using an equilibrium heat of fusion for PEO crystals (8.66 kJ/mol)[54] and was normalized to the PEO weight fraction in the PEO-*b*-PS samples. T_g^{PS} was identified as the midpoint of the stepwise increase of the heat capacity.

Bright-field (BF) imaging and electron diffraction (ED) were performed with a JEOL 1200EX transmission electron microscope (TEM) equipped with a rotating−tilting stage at an accelerating voltage of 120 kV. In order to determine the chain-folding direction in the lamellar crystals, a surface polyethylene (PE) decoration method was used.[55,56] A linear PE sample with a M_n^{PE} of 12K g/mol and polydispersity of 1.2 was used. A 10 cm distance between the sample and the basket was found to be optimal.

A Nanoscope III AFM (Digital Instruments/Veeco Metrology Group) equipped with a hot stage was used for morphological and stability analysis. The sample temperature was controlled via a thermocouple placed under the AFM sample holder. The temperature difference between the thermocouple and the sample was determined from the melting point of benzophenone ($T_m^0 = 48$ °C). The tapping mode was used to observe the morphology of the lamellar single crystals and to measure the overall thickness and the lateral size. On heating the sample in AFM, the morphological change of the single crystal lamella was captured in situ during the melting process of the crystals.

Shear force modulation AFM experiments were performed in a dry argon atmosphere using V-shaped contact-mode silicon cantilevers from Mikromasch (CSC21, 0.12 N/m). The piezoelectric scanner (E-type scanner) was modulated in the lateral direction by applying a small sinusoidal signal from an external generator, while the vertical deflection of the cantilever resulting from the interaction with the sample was kept constant using the feedback loop of the Nanoscope software. The optical response of the cantilever generated by the position sensitive photodiode was compared to the drive signal with the help of a dual-phase digital lock-in amplifier. The drive signal frequency (1.1 kHz) was chosen to be far from the resonant modes of the scanner. The amplitude of the driving signal was selected to be such that the AFM tip stayed constant in the static friction regime without sliding over the sample surface.

In order to obtain the individual thickness of the PEO layer and PS layer, we assume that the density of two PS nanolayers is identical to that of the amorphous PS bulk ($\rho_{PS} = 1.052$ g/cm^3); the densities of PEO crystal (ρ_{PEO}^c) and amorphous PEO (ρ_{PEO}^a) are 1.239 and 1.124 g/cm^3, respectively.[38] The PEO layer thickness, d_{PEO}, can thus be estimated from the overall thickness of the PS/PEO/PS system $d_{OVERALL}$ in a first-order approximation[51]

$$d_{PEO} = d_{OVERALL} \times \frac{M_n^{PEO}/(W_{PEO}^c \rho_{PEO}^c + W_{PEO}^a \rho_{PEO}^a)}{M_n^{PEO}/W_{PEO}^c \rho_{PEO}^c + W_{PEO}^a \rho_{PEO}^a + M_n^{PS}/\rho_{PS}} \quad (1)$$

and the PS layer thickness d_{PS} is calculated to be

$$d_{PS} = (d_{OVERALL} - d_{PEO})/2 \quad (2)$$

Results and Discussion

"Sandwiched" PEO-*b*-PS Lamellar Single Crystals. Figure 1 is a bright-field TEM image that shows a single crystal of PEO-*b*-PS diblock copolymer ($M_n^{PEO} = 11$K g/mol and $M_n^{PS} = 17$K g/mol) grown in chlorobenzene/octane mixed solution at $T_x = 30$ °C. The crystal is bounded by four (120) crystal planes. The corresponding ED pattern and indices of the most important diffraction spots are shown in the inset of Figure 1. This is the [001] zone diffraction pattern, and the *c*-axis of the crystal is parallel to the electron beam. The weak (110) and (020) spots lying in between the (120) spots indicate the crystal structure fits to the monoclinic lattice as discussed in previous publications.[48–51] The monoclinic unit cell of the PEO crystal

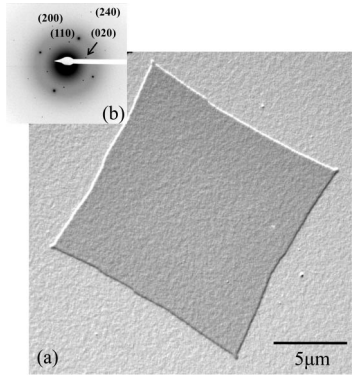

Figure 1. Bright-field TEM micrograph of a PEO-*b*-PS lamella grown at 30 °C in chlorobenzene/octane mixed dilute solution (a) and corresponding ED pattern of this PEO lamellar single crystal (b).

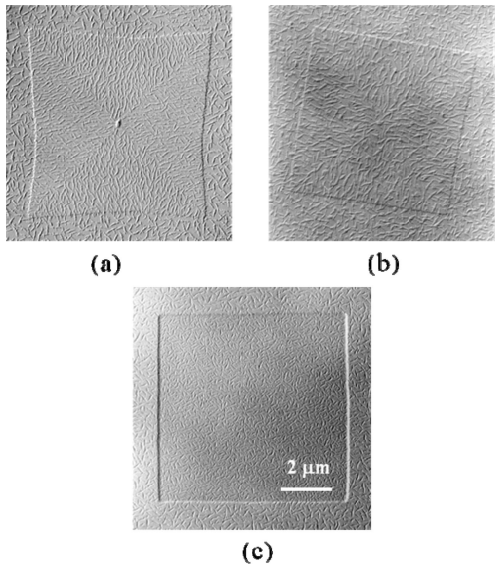

Figure 2. Set of bright-field TEM micrographs for a homo-PEO single crystal and PEO-*b*-PS diblock copolymer single crystals with different molecular weights. All of these single crystals were decorated with low molecular weight PE. (a) A homo-PEO single crystal with clear PE rod crystals oriented perpendicular to the (120) face in all four sectors. (b) A PEO-*b*-PS diblock copolymer with $M_n^{PS} = 3.8$K g/mol and $M_n^{PEO} = 67$K g/mol. There still exists some orientation of the PE rod crystals, indicating incomplete coverage by the PS blocks. (c) A PEO-*b*-PS diblock copolymer with $M_n^{PS} = 17$K g/mol and $M_n^{PEO} = 11$K g/mol. Here, complete PS block coverage can be assumed due to the lack of orientation in the PE rod crystals.

is defined by the parameters $a = 0.805$ nm, $b = 1.304$ nm, $c = 1.948$ nm, and $\beta = 125.4°$.[57]

In order to understand the chain folding along the PEO lamellar single crystals, Figure 2a shows a bright-field TEM image for a homo-PEO lamellar single crystal grown under the same conditions as shown in Figure 1 and subject to the PE decoration method. Many small PE crystal rods are preferentially oriented normal to the fold directions on the top surface of the homo-PEO single crystal. Since the *c*-axis of the PE crystal rod is perpendicular to the long axis of the rod, the PE chain direction is thus parallel to the (120) planes. This observation indicates that the PEO chain folding is along the (120) planes.[56] Furthermore, these four directional orientations of the decorated PE rod crystals highlight the existence of four sectors of the PEO single crystals, in each of which the chain folding direction is along the growth plane.

When the PE decoration is applied to the PEO-*b*-PS block copolymer crystals, different results are obtained depending on the PEO/PS ratios. When the molecular weight of PS block is low and that of the PEO block is high, the PE crystal rods can be at least partially oriented as shown in Figure 2b for a PEO-*b*-PS with $M_n^{PS} = 3.8$K g/mol and $M_n^{PEO} = 67$K g/mol. This observation indicates that some of the PEO folds are still not covered by the PS chains, and thus, these folds can induce the PE oligomer orientation. Comparing Figure 2b with Figure 2a, it is evident that the orientation of the PE crystal rods at the fold surface is substantially reduced for this block copolymer sample, even though the PS blocks only possess a molecular weight of 3.8K g/mol.

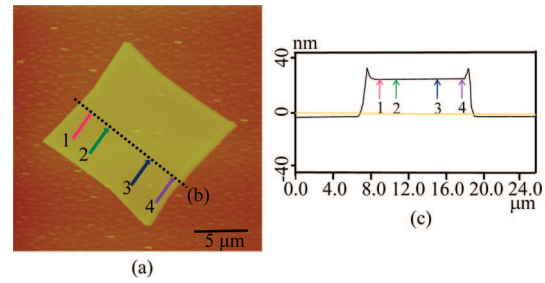

Figure 3. AFM image of a PEO-*b*-PS single crystal observed using the height mode (a), a measurement of average thickness of the PEO-*b*-PS single crystal (b), and a height profile of the single crystal (c).

As the molecular weight of the PS block increases and that of the PEO block decreases, only randomly oriented PE crystal rods can be observed, as shown in Figure 2c. Therefore, the PS blocks completely cover both the top and bottom basal surfaces of the PEO-*b*-PS single crystal. The PEO chain folds are buried underneath the PS layers, making the PE oligomers form randomly oriented crystal rods on the amorphous PS block surface.

The thickness and lateral size of the lamellae were measured in AFM for a PEO-*b*-PS single crystal with $M_n^{PEO} = 11$K g/mol and $M_n^{PS} = 17$K g/mol. The topography of a lamella crystallized at 30 °C is shown in Figure 3. This lamella has a lateral size of about 10 μm and an overall thickness, which includes one PEO single crystal layer sandwiched by two PS layers, of 22.3 nm. The lamellar surface is smooth (with a root-mean-square roughness of 0.2 nm), except for the edges of the single crystal. The lamellar thickness at the edge is observed, reproducibly, to be slightly thicker than the center. This is because near and at the edges the PS blocks have less covering area compared with those in the center as previously described.[50] On the basis of eqs 1 and 2, one can calculate that $d_{PEO} = 7.9$ nm and $d_{PS} = 7.2$ nm. Experimental observations of the d_{PEO} can also be carried out as described in previous publication.[50] The experimentally observed thickness data fit well with the calculated values based on eqs 1 and 2.

Transition Behavior of the PEO Single Crystal and Two Glassy PS Layers. The T_m^{PEO} of the PEO single crystal and T_g^{PS} of the PS layers are measured with DSC by using 1 mg of PEO-*b*-PS single crystal mats with $M_n^{PEO} = 11$K g/mol and $M_n^{PS} = 17$K g/mol at $T_x = 30$ °C in the mixed dilute solution. Figure 4 shows a sharp endotherm peak with a T_m^{PEO} of 56.5 °C observed for the PEO crystal melting in the PEO-*b*-PS "sandwiched" lamellae. Using the heat of fusion data in Figure 4, the calculated crystallinity is ~90%. The heat capacity increase at the T_g^{PS} can be seen in an enlarged DSC diagram in the inset of Figure 4. Even though the T_g^{PS} range is broader and the heat capacity increase, ΔC_p, at T_g^{PS} is weaker compared to the bulk PS as commonly reported,[41] this diagram clearly shows that T_g^{PS} is around 71 °C.

The T_g^{PS} can also be assessed by observing a change in surface topography of the glassy PS layer by in situ AFM

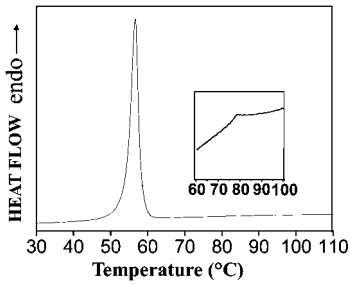

Figure 4. DSC melting thermal diagram for a PEO-*b*-PS sample which was collected by a large number of single crystals grown at 30 °C in chlorobenzene/octane mixed dilute solution. The insert is an enlarged DSC diagram in the T_g^{PS} region.

experiments at a slow heating rate of about 1 °C/min. The lamellar shape and thickness remain unchanged for at least 10 min when the temperature reaches 65 °C, as shown in Figure 5, although at this temperature the PEO single crystal is molten. When the temperature is further increased to the T_g^{PS} of the PS layers, about 70 °C, several small holes are initiated in the central part of the square-shaped PS layer surface. The onset of this change of the surface topography of the PS layer indicates that the glassy PS layers start to devitrify. Upon further increase of the temperature, the hole size continues to increase together with the formation of holes at the edges of the PS layers where they are relatively thicker. Figure 6 shows a series of TEM bright-field images for the samples that parallel the AFM images in Figure 5. In this case, the crystals were heated to different temperatures as indicated in the figure and kept there for 10 min, a residence time longer than in Figure 5, and quenched to room temperature for TEM sample preparation. Again, the hole formation is evident at 70 °C. ED patterns indicate that up to 50 °C the PEO single crystal lattice is maintained. At 60 °C, no diffraction is observed, indicating that the PEO single crystal has melted and that it does not recrystallize during subsequent sample preparations and observation at room temperature.

We also utilized the surface shear modulation AFM technique to determine the T_m^{PEO} and T_g^{PS}. This technique was used in the past to measure the glass transition temperature of thin supported layers.[58,59] The principal idea of this method consists of applying a small sinusoidal lateral drive signal to the piezoelectric scanner while keeping the AFM tip in contact with the sample. The mechanical response of the cantilever can then be measured by locking the signal from the corresponding quadrants of the position-sensitive photodiode at the frequency of the drive signal. Within the range of the detector linearity, the response signal is proportional to the dynamic amplitude of the cantilever deformation induced by the drive signal. In a simple mechanical model describing the contact mechanics of the tip−sample interaction in the surface shear modulation AFM experiments[57] as a system of two Voigt elements, the total deformation of the system imposed by the amplitude of the piezo-oscillation can be represented as a sum of the deformations of the cantilever and that of the contact area. Therefore, decreasing the spring constant of the tip−sample contact results in a decrease of the cantilever amplitude because more deformation is taken up by the sample. In practice, the glass transition temperature measurement of thin polymer layers measured with surface shear modulation AFM shows a result which is in apparent contradiction to this expectation; i.e., the dynamic amplitude of the cantilever oscillation increases across the transition. This can be explained by the fact that the tip−sample stiffness is a function not only of the sample modulus but also of the tip−sample area, which can dramatically increase when the AFM tip penetrates the softening sample.

Evaluation of the thermal transitions of PEO-*b*-PS lamellar single crystals studied with surface shear modulation AFM requires that very soft contact mode tips are applied to minimize damage to the sample. In the experiments, the normal force exerted on the lamellar surface by the tip does not exceed 10 nN, which makes it possible to keep the integrity of the lamellae even after several successive measurements in the same area. Typical results of these measurements are shown in Figure 7. Both curves display a characteristic increase of the dynamic amplitude of the cantilever response with temperature. We have found two different transition temperatures by this method: the lower one is at about 57 °C and the higher one at ~71 °C. 57 °C corresponds to the T_m^{PEO} of the PEO block, while 71 °C most probably reflects the T_g^{PS}. Interestingly enough, each of the curves shows only one transition.

We tried to understand why in some cases the glass transition temperature of the PS blocks is not visible, whereas one would logically expect to have it on all of the curves since the PS blocks entirely cover the surface of the crystals. As shown in Figures 4 and 6, the melting point of the PEO block manifests itself as both the endothermic process in DSC and disappearance of the single crystal diffraction pattern. It is noteworthy that the thickness of this region is relatively smaller than the thickness of the edges, which could explain why the less dense PS brush in this region cannot keep the integrity of the molten PEO blocks. Therefore, the temperature where the holes start to appear should be an onset of the glass transition of the PS layers. Upon further heating, the number and size of holes increased, whereby the rate of this increase dramatically accelerated above 70 °C, namely, in the supposed range of the PS glass transition temperature. It is possible that the amplitude curves showing only the lower temperature transition correspond to a situation where the tip is trapped in one of the forming holes and becomes insensitive to the glass transition temperature of PS blocks. Conversely, when the tip stays on the peripheral part of the crystal, the melting transition of PEO blocks is not sensed probably due to a relatively small thickness of the PEO layer. Note that compared to previous measurements[58] the thickness of the films used in the present work is smaller. This may explain why the amplitude curves reach saturation level shortly after the transition temperature: the contact area cannot increase further because the tip penetrates the layer down to the substrate.

The DSC, AFM, and TEM results provide identical values of T_m^{PEO} = 57 °C and T_g^{PS} = 71 °C for the PEO-*b*-PS copolymer. The onset of the glass transition is approximately between 65 and 70 °C from DSC. Thus, the PS layer confinement can be sustained up to at least 63 °C. This temperature is high enough to melt the PEO single crystals while retaining PS glassy layers, creating a molten PEO layer in 1D nanoconfinement. We can then perform isothermal recrystallization of the PEO blocks at different T_{rx} values with or without the self-seeding procedure.

PEO Block Recrystallization Behavior within Two Glassy PS Layers. On the basis of the above T_m^{PEO} and T_g^{PS} data, the PEO single crystal layer can be melted at 63 °C for 5 min below the T_g^{PS} and recrystallized at a lower T_{rx} under a 1D confinement generated by the two rigid thin layers of the PS block. Figure 8a is the ED pattern of the PEO-*b*-PS lamella kept at T_{rx} = 5 °C for 8 days after the sample was kept at 63 °C for 5 min. The ED pattern displays only diffuse amorphous rings. The same patterns were observed when the lamellae were tilted at different angles along different directions. This observation indicates that the PEO layer confined in between two PS layers cannot crystallize at 5 °C for the prolonged period (e.g., 8 days). The question is whether keeping the sample at 5 °C for 8 days will affect the PEO block recrystallization behavior when the samples are further quenched to lower T_{rx} values such as −40 °C. We then quenched the sample to T_{rx} = −40 °C and kept it there

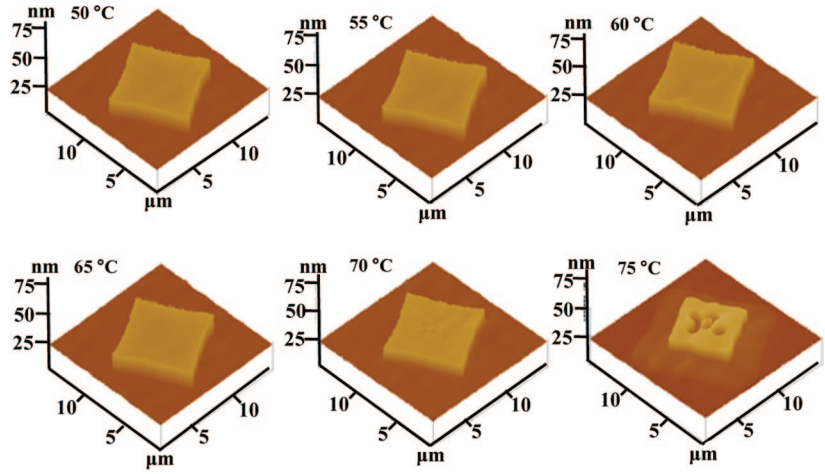

Figure 5. In situ topographic change of a PEO-*b*-PS single crystal observed in AFM height mode during heating at different temperatures.

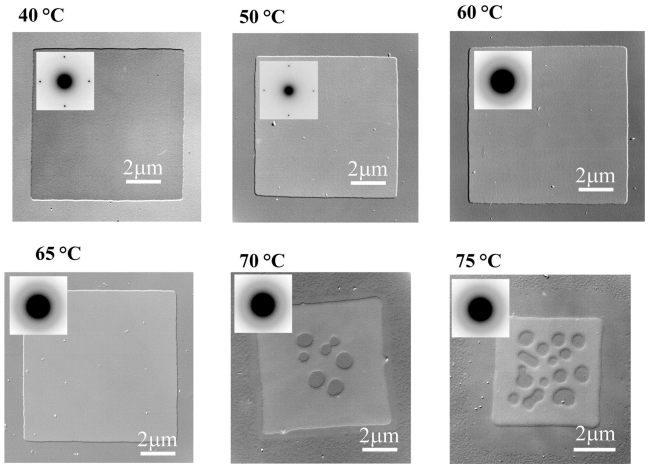

Figure 6. Set of TEM bright-field images of the PEO-*b*-PS single crystals after they were annealed at different temperatures and then quenched to room temperature. The inset in each BF image is the corresponding ED pattern.

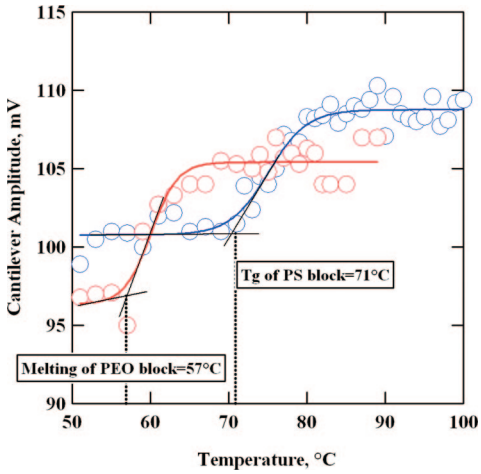

Figure 7. Temperature dependence of the dynamic amplitude of the cantilever as a function of temperature. The curves show characteristic transitions which can be assigned to the melting temperature of the PEO block and glass transition temperature of the PS block.

for 2 h. Figure 8b shows an ED pattern which exhibits two isotropic diffraction rings (see below for detailed assignments), indicating that the PEO blocks have been recrystallized.

We have also conducted experiments by directly quenching the PEO-*b*-PS single lamellae samples to $T_{rx} = -40$ °C after

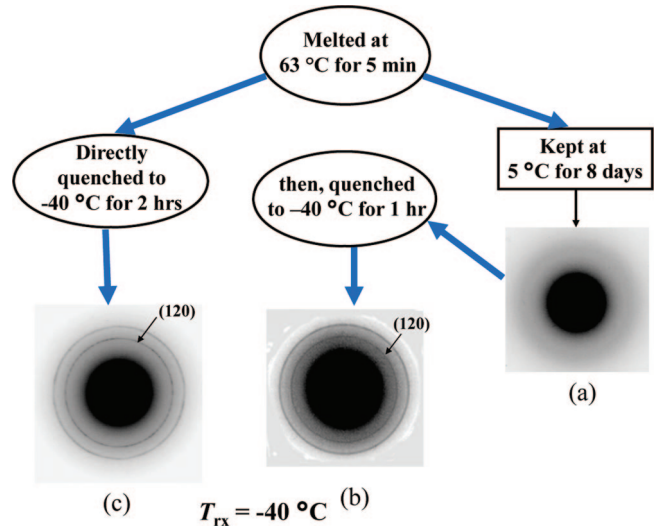

Figure 8. ED pattern of a PEO-*b*-PS lamella after melting the PEO single crystal at 63 °C for 5 min and recrystallization at $T_{rx} = 5$ °C for 8 days (a). ED pattern for the same sample after staying at $T_{rx} = 5$ °C for 8 days, then quenching to −40 °C, and returning to room temperature (b). ED pattern of the sample that was directly quenched to −40 °C after staying at 63 °C for 5 min (c).

the samples were melted at 63 °C for 5 min. The sample was kept there isothermally for 2 h. Figure 8c is an ED pattern obtained after this sample treatment; comparing Figure 8c to Figure 8b, both ED patterns exhibit identical PEO crystal diffractions. This observation indicates that the PEO blocks do not have any memory in the melt from their previous thermal treatment, and they remain in the metastable state when quenched to 5 °C for 8 days.

Recrystallization of the PEO blocks occurring at such a low temperature is surprising. Indeed, it is known that for the bulk 1D lamellar confinement obtained via mechanical shear crystallization takes place around 27 °C as determined by DSC for a cooling rate of 5 °C/min.[41] For a PEO homopolymer and identical cooling rate, crystallization takes place around 50 °C.[60] By contrast, in the present case of the PEO blocks in a "sandwiched" lamellar confinement, crystallization does not take place even at $T_{rx} = 5$ °C. This observation indirectly demonstrates that the defects in the bulk 1D confinement substantially affect the PEO block crystallization kinetics by releasing the confinement and significantly increasing the crystallization temperature during cooling via a heterogeneous nucleation process. The observation reflected in Figure 8a,c confirms that

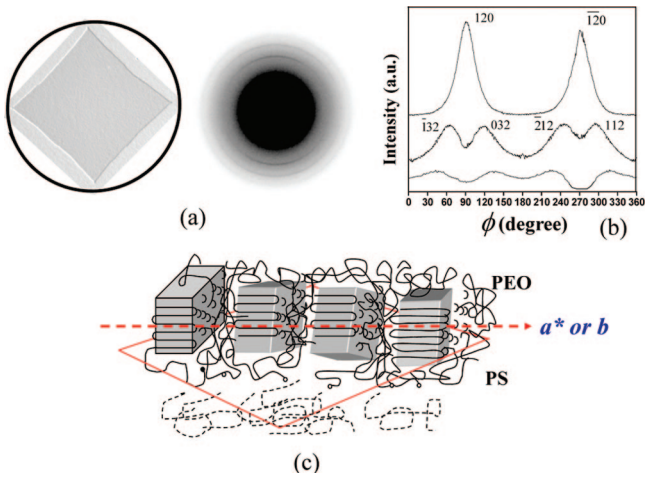

Figure 9. Lamellar morphology and ED pattern of the recrystallized PEO blocks at $T_{rx} = -20$ °C (a), the azimuthal profiles of the diffractions (b), and the crystal orientation illustrated by a schematic drawing (c).

the PEO block crystallization in this PEO-*b*-PS lamella takes place in a 1D defect-free confinement.

T_{rx} Dependence of PEO Crystal Orientation Observed via the ED Technique. WAXD has been used to determine the PEO crystal orientation dependence on crystallization temperature in mechanically sheared diblock copolymer bulk samples.[26,30–34,37] Since lamellar single crystals of PEO-*b*-PS are grown in dilute solution, we resort to the ED technique to study microscopic crystal orientation after confined recrystallization in the lamellae. When $-50\ °C \le T_{rx} < -20\ °C$, the ED pattern of the recrystallized lamellar sample exhibits two major diffraction rings, as shown in Figure 8b,c. The inner ring with a *d*-spacing of 0.463 nm is indexed as (120), while the outer ring consists of overlapped (032), (112), ($\bar{1}$32), and ($\bar{2}$12) diffractions with a *d*-spacing of 0.39 nm. This pattern is observed even after using a rotating-tilt stage. The PEO block crystals are thus randomly oriented in this 7.9 nm thick layer, and the crystal size is significantly smaller than 7.9 nm.

Figure 9a shows a typical ED pattern which was taken from an entire PEO-*b*-PS lamella recrystallized at T_{rx} between −20 and −5 °C. The pattern and the lamellar PEO-*b*-PS single crystal are in the correct orientation. The ED pattern exhibits interesting features. The arcs observation (rather than rings) indicates that the PEO crystals have a fair degree of orientation. The azimuthal profile of inner (120) diffraction in Figure 9a shows that diffraction arcs are along the diagonal direction of the square lamella (Figure 9b). The next two pairs of diffractions represent the overlapped (1$\bar{1}$2), (0$\bar{3}$2), ($\bar{2}$12), and ($\bar{1}$32) diffractions in Figure 9a. Their azimuthal profile indicates that they are ±23° away from the (120) pair axis (Figure 9b). The outermost pairs of diffraction arcs (*d*-spacing 0.33−0.34 nm) are weak. Their azimuthal profile indicates that they are ±47° away from the (120) pair axis (Figure 9b). These arcs can be indexed as (0$\bar{2}$4) and ($\bar{2}$24). Note that when the (0$\bar{2}$4), ($\bar{2}$24), (1$\bar{2}$0), and ($\bar{1}$20) reflection are all present in the ED pattern, this zone axis is [421].[57,61] This axis is normal to the *c*-axis or chain direction. Otherwise, it is a *c*-axis fiber pattern-like ED pattern.[26] The chain direction in the crystals is, therefore, parallel to the lamellar surface. As a result, the ED pattern in Figure 9 is most likely a PEO crystal ED fiber pattern. The *c*-axis is always perpendicular to the lamellar normal and aligns along either the *a**-(*a* sin β) or *b*-axis of the original single crystals, as illustrated in the schematics given in this figure.

As shown in Figure 8, when $T_{rx} = 5$ °C, the PEO blocks do not crystallize even after a prolonged time period of 8 days. In

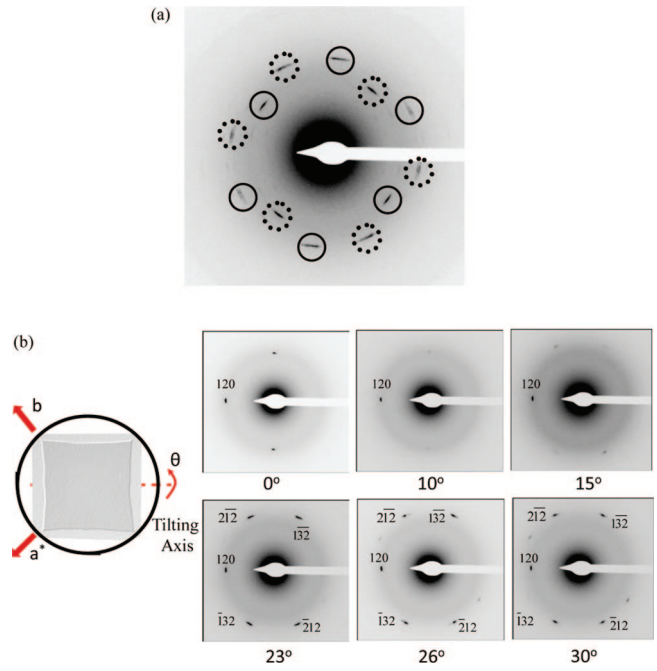

Figure 10. ED patterns of the recrystallized PEO at $T_{rx} = 30$ °C after self-seeding. Two sets of ED patterns are identified by solid and dash circles (a) and six ED patterns of a PEO-*b*-PS single crystal taken from different tilting angles with respect to the (120) normal (b).

fact, the upper limit T_{rx} of the PEO blocks after they were melted at 63 °C is −5 °C. Note that the temperature where the homogeneous nucleation takes place for PEO crystallization in the bulk state is approximately −5 °C.[10,11,62,63] Therefore, we need to utilize the self-seeding procedure at $T_{rx} > -5$ °C. Figure 10a shows an ED pattern taken over the entire single crystal after the PEO blocks were recrystallized at $T_{rx} = 30$ °C after self-seeding. The ED pattern differs remarkably with the PEO single crystal pattern shown in Figure 1. In Figure 10a, in addition to the (120) reflections, four outer pairs of reflections with a *d*-spacing of 0.39 nm, which are the (1$\bar{1}$2), (0$\bar{3}$2) [or ($\bar{1}$32) and ($\bar{2}$12)] spots, appear. These four outer pairs of diffractions should not be present if Figure 10a is a pure [001] zone ED pattern. Therefore, this ED pattern should consist of two superimposed sets of ED patterns. The judgment of this ED pattern is further confirmed by TEM tilting experiment of a PEO-*b*-PS single crystal with the (120) normal as the tilting axis, as seen in Figure 10b. ED pattern evolution with increased tilting angle shows that the pair of (1$\bar{2}$0) spots starts to disappear with increasing tilting angle between 5° and 10°. Two additional (*hk*2) pairs such as ($\bar{1}$32)/(1$\bar{3}\bar{2}$) and ($\bar{2}$12)/(2$\bar{1}\bar{2}$) clearly appear (indexed in the figure) by the tilting angle from 23° to 30°. The identical pattern contributed from one set of PEO polycrystals (Figure 10a) and single crystal with specific tilting angles (Figure 10b) indicates that the monoclinic unit cell of the PEO block in 1D confined crystallization is maintained. From this experiment, it is evident that two sets of superimposed ED patterns shown in Figure 10a are associated with PEO chain inclination measured to be 26°, and their inclined directions are perpendicular to each other. Each of these two patterns makes of one pair of (120) reflections, pairs of the ($\bar{1}$32)/(1$\bar{3}\bar{2}$) and ($\bar{2}$12)/(2$\bar{1}\bar{2}$) for the [4$\bar{2}$5] zone, and another two pairs of the (112)/($\bar{1}\bar{1}\bar{2}$) and (032)/(0$\bar{3}\bar{2}$) for the [42$\bar{3}$] zone, as shown in Figure 11. This indicates that the *c*-axis (the chain direction) of the PEO crystals is tilted from the lamellar normal, approximately by 26° along the perpendicular directions. We speculate that this orthogonal relation between these two tilting directions is due possibly to the effect of the chain-folding direction of the

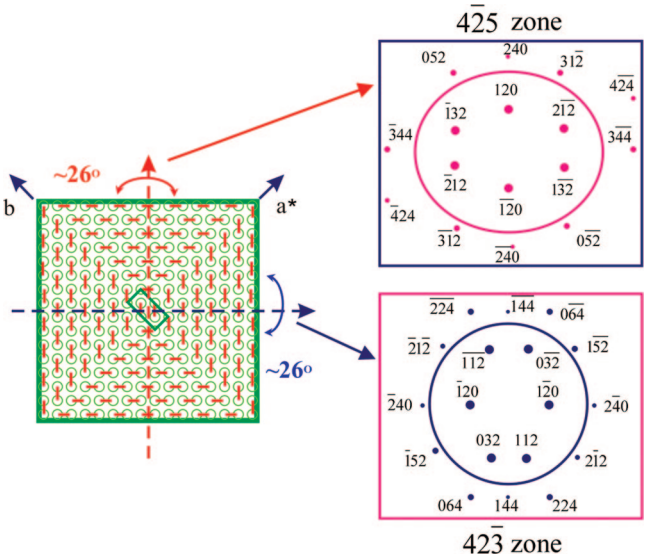

Figure 11. Detailed analysis of these two superimposed ED patterns.

original PEO single crystals in each of the four sectors. However, experimental confirmation is still to come.

Conclusion

We have created a defect-free, 1D nanoconfinement by growing single crystals of PEO-*b*-PS block copolymers in dilute solution. On the basis of different characterization methods, it has been shown that for a PEO-*b*-PS with $M_n^{PEO} = 11$k g/mol and $M_n^{PS} = 17$k g/mol, the T_m of the PEO single crystal layers is 57 °C, and the T_g of the thin PS glass layers is 71 °C in lamellar single crystals. Then, it is possible to melt the PEO single crystals, keeping the thin PS layers in the glassy state. Therefore, a defect-free nanoscale confined lamella can be achieved by the path of quenching the lamellar sample down to different isothermal T_{rx} to recrystallize the PEO blocks. Using this approach, we can obtain knowledge on how a perfect 1D confined environment affects polymer chain crystallization. In this system, the issue of phase-structure defects introduced by using bulk lamellar diblock copolymers via mechanical shear can be avoided. However, commonly used WAXD experiments are no longer applicable here to determine crystallization of PEO blocks within this defect-free confined space. Instead, the ED technique in TEM has to be utilized to investigate crystallization kinetics and the *c*-axis orientation of the PEO block crystals. Our results show that PEO crystallization kinetics in this specially designed 1D confined lamella is substantially hampered. The crystallization process can proceed only in a temperature region below the temperature where homogeneous nucleation takes place ($T_{rx} = -5$ °C).

In this study, we have also demonstrated that the orientation of the *c*-axis of the recrystallized PEO blocks in two thin PS glass layers changes with the T_{rx}. They possess a random *c*-axis orientation when $T_{rx} < -20$ °C, where the crystal sizes are three-dimensionally small. When -20 °C $\leq T_{rx} < -5$ °C, the *c*-axis is parallel to the lamellar basal plane and aligns with the *a**- or *b*-axis of the original PEO-*b*-PS single crystal. Finally, when $T_{rx} > -5$ °C, the *c*-axis starts to approach the lamellar normal with a tilted angle of 26°. In order to completely understand the chain orientation in Figure 9a and the two overlapped ED patterns in Figure 10a, we need selected area ED patterns and dark-field images from each original sector of the lamellar single crystal sample. Also, investigation of the PEO chain orientation of the newly formed crystals (which is no longer a single crystal) in each sector should be determined in order to recognize the cause of the formation of those two unique crystal orientations. We are currently making progress along these research directions, and they will be reported in the near future.

Acknowledgment. This work was supported by NSF (DMR-0516602). We also acknowledge Perkin-Elmer Co. for providing a Diamond DSC instrument for our laboratory.

References and Notes

(1) Dadmuna, M. D.; Muthukumar, M. *J. Chem. Phys.* **1993**, *98*, 4850.
(2) Keddie, J. L.; Jones, R. A. L.; Cory, R. A. *Europhys. Lett.* **1994**, *27*, 59.
(3) Ogata, N.; Kawakage, S.; Ogihara, T. *Polymer* **1997**, *38*, 5115.
(4) Giannelis, E. P.; Krishnamoorti, R.; Manias, E. *Adv. Polym. Sci.* **1999**, *138*, 107.
(5) Jiang, C. H.; Zhang, G. L.; Zhang, H. Z.; Qi, Z. N. *Acta Polym. Sin.* **1999**, *6*, 765.
(6) Park, J.-Y.; McKenna, G. B. *Phys. Rev. B* **2000**, *61*, 6667.
(7) Loo, Y. L.; Register, R. A.; Ryan, A. J. *Phys. Rev. Lett.* **2000**, *84*, 4120.
(8) Zhu, L.; Chen, Y.; Zhang, A.; Calhoun, B. H.; Chun, M.; Quirk, R. P.; Cheng, S. Z. D.; Hsiao, B. S.; Yeh, F.; Hashimoto, T. *Phys. Rev. B* **1999**, *60*, 10022.
(9) Li, C. Y.; Ge, J. J.; Bai, F.; Calhoun, B. H.; Harris, F. W.; Cheng, S. Z. D.; Chien, L.-C.; Lotz, B.; Keith, H. D. *Macromolecules* **2001**, *34*, 3634.
(10) Massa, M. V.; Carvalho, J. L.; Dalnoki-veress, K. *Eur. Phys. J. E* **2003**, *12*, 111.
(11) Massa, M. V.; Dalnoki-Veress, K. *Phys. Rev. Lett.* **2004**, *92*, 255509.
(12) Ellison, C. J.; Mundra, M. K.; Torkelson, J. M. *Macromolecules* **2005**, *38*, 1767.
(13) Alcoutlabi, M.; McKenna, G. B. *J. Phys.: Condens. Matter* **2005**, 17R461.
(14) Woo, E.; Huh, J.; Jeong, Y. G.; Shin, K. *Phys. Rev. Lett.* **2007**, *98*, 136103.
(15) Bates, F. S.; Fredrickson, G. H. *Annu. Rev. Phys. Chem.* **1990**, *41*, 525.
(16) Hamley, I. W. *The Physics of Block Copolymers*; Oxford University Press: New York, 1998.
(17) Cohen, R. E.; Cheng, P. L.; Douzinas, K. C.; Kofinas, P.; Berney, C. V. *Macromolecules* **1990**, *23*, 324.
(18) Douzinas, K. C.; Cohen, R. E. *Macromolecules* **1992**, *25*, 5030.
(19) Sakurai, K.; MacKnight, W. J.; Lohse, D. J.; Schulz, D. N.; Sissano, J. A. *Macromolecules* **1993**, *26*, 3236.
(20) Cohen, R. E.; Bellare, A.; Drzewinski, M. A. *Macromolecules* **1994**, *27*, 2321.
(21) Khandpur, A. K.; Macosko, C. W.; Bates, F. S. *J. Polym. Sci., Polym. Phys. Ed.* **1995**, *33*, 247.
(22) Hamley, I. W.; Fairclough, J. P. A.; Ryan, A. J.; Bates, F. S.; Towns-Andrews, E. *Polymer* **1996**, *37*, 4425.
(23) Zhao, J.; Majumdar, B.; Schulz, M. F.; Bates, F. S.; Almdal, K.; Mortensen, K.; Hajduk, D. A.; Gruner, S. M. *Macromolecules* **1996**, *29*, 1204.
(24) Liu, L. Z.; Yeh, F.; Chu, B. *Macromolecules* **1996**, *29*, 5336.
(25) Hamley, I. W.; Fairclough, J. P. A.; Terrill, N. J.; Ryan, A. J.; Lipic, P. M.; Bates, F. S.; Towns-Andrews, E. *Macromolecules* **1996**, *29*, 8835.
(26) Zhu, L.; Cheng, S. Z. D.; Calhoun, B. H.; Ge, Q.; Quirk, R. P.; Thomas, E. L.; Hsiao, B. S.; Yeh, F.; Lotz, B. *J. Am. Chem. Soc.* **2000**, *122*, 5957.
(27) Zhu, L.; Calhoun, B. H.; Chun, M.; Quirk, R. P.; Cheng, S. Z. D.; Thomas, E. L.; Lotz, B.; Hsiao, B. S.; Yeh, F.; Liu, L. *Macromolecules* **2001**, *34*, 1244.
(28) Park, C.; De Rosa, C.; Fetters, L. J.; Thomas, E. L. *Macromolecules* **2000**, *33*, 7931.
(29) Loo, Y. L.; Register, R. A.; Adamson, D. H. *Macromolecules* **2000**, *33*, 8361.
(30) Huang, P.; Zhu, L.; Cheng, S. Z. D.; Ge, Q.; Quirk, R. P.; Thomas, E. L.; Lotz, B.; Hsiao, B. S.; Liu, L.; Yeh, F. *Macromolecules* **2001**, *34*, 6649.
(31) Zhu, L.; Cheng, S. Z. D.; Huang, P.; Ge, Q.; Quirk, R. P.; Thomas, E. L.; Lotz, B.; Hsiao, B. S.; Yeh, F.; Liu, L. *Adv. Mater.* **2002**, *14*, 31.
(32) Zhu, L.; Huang, P.; Chen, W. Y.; Ge, Q.; Quirk, R. P.; Cheng, S. Z. D.; Thomas, E. L.; Lotz, B.; Hsiao, B. S.; Yeh, F.; Liu, L. *Macromolecules* **2002**, *35*, 3553.
(33) Huang, P.; Zhu, L.; Guo, Y.; Ge, Q.; Jing, A. J.; Chen, W. Y.; Quirk, R. P.; Cheng, S. Z. D.; Thomas, E. L.; Lotz, B.; Hsiao, B. S.; Avila-Orta, C. A.; Sics, I. *Macromolecules* **2004**, *37*, 3689.
(34) Huang, P.; Guo, Y.; Quirk, R. P.; Ruan, J.; Lotz, B.; Thomas, E. L.; Hsiao, B. S.; Avila-Orta, C. A.; Sics, I.; Cheng, S. Z. D. *Polymer* **2006**, *47*, 5457.

(35) Sun, Y. S.; Chung, T. M.; Li, Y. J.; Ho, R. M.; Ko, B. T.; Jeng, U. S.; Lotz, B. *Macromolecules* **2006**, *39*, 5782.
(36) Sun, Y. S.; Chung, T. M.; Li, Y. J.; Ho, R. M.; Ko, B. T.; Jeng, U. S.; Lotz, B. *Macromolecules* **2007**, *40*, 6781.
(37) Huang, P.; Zheng, J. X.; Leng, S.; Van Horn, R. M.; Jeong, K. U.; Guo, Y.; Quirk, R. P.; Cheng, S. Z. D.; Lotz, B.; Thomas, E. L.; Hsiao, B. S. *Macromolecules* **2007**, *40*, 526.
(38) Wunderlich, B. *Macromolecular Physics*; **1973**; Vol. *I*, Chapter 4.
(39) Gido, S. P.; Thomas, E. L. *Macromolecules* **1994**, *27*, 6137.
(40) Marencic, A. P.; Wu, M. W.; Register, R. A.; Chaikin, P. M. *Macromolecules* **2007**, *40*, 7299.
(41) Zhu, L.; Cheng, S. Z. D.; Calhoun, B. H.; Ge, Q.; Quirk, R. P.; Thomas, E. L.; Hsiao, B. S.; Yeh, F.; Lotz, B. *Polymer* **2001**, *42*, 5829.
(42) Lvov, Y.; Ariga, K.; Ichinose, I.; Kunitake, T. *Thin Solid Films* **1996**, *284−285*, 797.
(43) Vierheller, T. R.; Foster, M. D.; Schmidt, A.; Mathauer, K.; Knoll, W.; Wegner, G.; Satijia, S.; Majkrzak, C. F. *Macromolecules* **1994**, *27*, 6893.
(44) Yamamoto, S.; Tsujii, Y.; Yamada, K.; Fukuda, T.; Miyamoto, T.; Ito, S. *Langmuir* **1996**, *12*, 3671.
(45) Reiter, G. *Macromolecules* **1994**, *27*, 3046.
(46) Limary, R.; Green, P. F. *Macromolecules* **1999**, *32*, 8167.
(47) Smith, M. D.; Green, P. F.; Saunders, R. *Macromolecules* **1999**, *32*, 8392.
(48) Lotz, B.; Kovacs, A. J.; Bassett, G. A.; Keller, A. *Kolloid Z. Z. Polym.* **1966**, *209*, 115.
(49) Chen, W. Y.; Zheng, J. X.; Cheng, S. Z. D.; Li, C. Y.; Huang, P.; Zhu, L.; Xiong, H.; Ge, Q.; Guo, Y.; Quirk, R. P.; Lotz, B.; Deng, L.; Wu, C.; Thomas, E. L. *Phys. Rev. Lett.* **2004**, *93*, 028301.
(50) Chen, W. Y.; Li, C. Y.; Zheng, J. X.; Huang, P.; Zhu, L.; Ge, Q.; Quirk, R. P.; Lotz, B.; Deng, L.; Wu, C.; Thomas, E. L.; Cheng, S. Z. D. *Macromolecules* **2004**, *37*, 5292.
(51) Zheng, J. X.; Xiong, H.; Chen, W. Y.; Lee, K.; Van Horn, R. M.; Quirk, R. P.; Lotz, B.; Thomas, E. L.; Shi, A.-C.; Cheng, S. Z. D. *Macromolecules* **2006**, *39*, 641.
(52) Quirk, R. P.; Kim, J.; Kausch, C.; Chun, M. S. *Polym. Int.* **1996**, *39*, 3.
(53) Lotz, B.; Kovacs, A. J. *Kolloid Z. Z. Polym.* **1966**, *209*, 97.
(54) Cheng, S. Z. D.; Wunderlich, B. *J. Polym. Sci., Polym. Phys. Ed.* **1986**, *24*, 577.
(55) Wittmann, J. C.; Lotz, B. *J. Polym. Sci., Polym. Phys. Ed.* **1985**, *23*, 205.
(56) Chen, J.; Cheng, S. Z. D.; Wu, S. S.; Lotz, B.; Wittmann, C. C. *J. Polym. Sci., Polym. Phys. Ed.* **1995**, *33*, 1851.
(57) Takahashi, Y.; Tadokoro, H. *Macromolecules* **1973**, *6*, 672.
(58) Ge, S.; Pu, Y.; Zhang, W.; Rafailovich, M.; Sokolov, J.; Buenviaje, C.; Buckmaster, R.; Overney, R. M. *Phys. Rev. Lett.* **2000**, *85*, 2340.
(59) Pu, Y.; Ge, S.; Rafailovich, M.; Sokolov, J.; Duan, Y.; Pearce, E.; Zaitsev, V.; Schwarz, S. *Langmuir* **2001**, *17*, 5865.
(60) Cheng, S. Z. D.; Barley, J. S.; Zhang, A.; Habenschuss, A.; Zschack, P. R. *Macromolecules* **1992**, *25*, 1453.
(61) Tadokoro, H.; Chatani, Y.; Yoshihara, T.; Tahara, S.; Murahashi, S. *Makromol. Chem.* **1964**, *73*, 109.
(62) Cormia, R. L.; Price, F. P.; Turnbull, D. *J. Chem. Phys.* **1962**, *37*, 1333.
(63) Koutsky, J. A.; Walton, A. G.; Baer, E. *J. Appl. Phys.* **1967**, *38*, 1832.

MA8006619